Development 134, 167-176 (2007) doi:10.1242/dev.02701

Dusp6 (*Mkp3*) is a negative feedback regulator of FGF-stimulated ERK signaling during mouse development

Chaoying Li[1], Daryl A. Scott[1,*], Ekaterina Hatch[1], Xiaoyan Tian[2] and Suzanne L. Mansour[1,†]

Mitogen-activated protein kinase (MAPK) pathways are major mediators of extracellular signals that are transduced to the nucleus. MAPK signaling is attenuated at several levels, and one class of dual-specificity phosphatases, the MAPK phosphatases (MKPs), inhibit MAPK signaling by dephosphorylating activated MAPKs. Several of the MKPs are themselves induced by the signaling pathways they regulate, forming negative feedback loops that attenuate the signals. We show here that in mouse embryos, Fibroblast growth factor receptors (FGFRs) are required for transcription of *Dusp6*, which encodes MKP3, an extracellular signal-regulated kinase (ERK)-specific MKP. Targeted inactivation of *Dusp6* increases levels of phosphorylated ERK, as well as the pERK target, *Erm*, and transcripts initiated from the *Dusp6* promoter itself. Finally, the *Dusp6* mutant allele causes variably penetrant, dominant postnatal lethality, skeletal dwarfism, coronal craniosynostosis and hearing loss; phenotypes that are also characteristic of mutations that activate FGFRs inappropriately. Taken together, these results show that DUSP6 serves in vivo as a negative feedback regulator of FGFR signaling and suggest that mutations in *DUSP6* or related genes are candidates for causing or modifying unexplained cases of FGFR-like syndromes.

KEY WORDS: *Mkp3*, *Pyst1*, Dual specificity phosphatase, Craniosynostosis, Middle ear, Otic capsule, Mouse

INTRODUCTION

Fibroblast growth factors (FGFs) comprise a family of small, highly basic proteins that typically are secreted and bind to and activate high-affinity FGF receptors (FGFRs), a family of single-pass transmembrane proteins with intracellular tyrosine kinase activity. FGF signals are transduced to cellular targets by several distinct intracellular signaling pathways. Cells respond to FGF signals in a context-dependent manner; in different instances they may be stimulated to divide, to differentiate, to migrate or to survive. Loss-of-function genetic studies are beginning to reveal the ways in which these FGF-dependent cell behaviors are deployed during the development of many different organs (Itoh and Ornitz, 2004; Thisse and Thisse, 2005). The responses to FGF signals are dose-dependent. Just as a reduction in FGF signals can lead to developmental abnormalities, so too does an increase in FGF signaling. Indeed, some of the most frequently observed human mutations are activating mutations in *Fgfr* genes that cause a variety of dominant skeletal disorders (Cohen, 2004; Wilkie, 2005).

Many FGF signals travel and are amplified through the extracellular-signal-regulated kinase (ERK) mitogen-activated protein kinase (MAPK) pathway. FGF binding stimulates autophosphorylation of the FGFR, which recruits signal adapters and leads to sequential phosphorylation and activation of cytoplasmic protein kinases, ultimately resulting in the diphosphorylation of ERK on threonine and tyrosine residues. This activated form of ERK has substrates in all cellular compartments, including the nucleus, where it phosphorylates and activates transcription factors, effecting changes in gene expression (Powers et al., 2000; Chen et al., 2001; Tsang and Dawid, 2004; Eswarakumar et al., 2005). Significantly, Corson and colleagues (Corson et al., 2003) showed that most of the diphosphorylated ERK (dpERK, an indicator of ERK pathway activity) in early mouse embryos [embryonic day (E) 6.5-10.5] is dependent on FGFR activity. This suggests that FGFs, as opposed to other signals that also act through receptor tyrosine kinases, are the major input into the ERK pathway at these stages.

Signaling through MAPK pathways can be attenuated at several levels and one class of dual-specificity phosphatases, the MAPK phosphatases (MKPs) inhibit MAPK signaling by dephosphorylating activated MAPKs. For example, in *Saccharomyces cerevisiae*, mating pheromone-induced signaling through the MAPK Fus3p induces the MKP Msg5p, which feeds back to turn off the signal by inactivating Fus3p (Zhan et al., 1997). Similarly, during *Drosophila* embryogenesis, signals required for dorsal closure activate the DJNK (basket) MAPK pathway, leading to transcriptional induction of the MKP puckered, which feeds back to inactivate DJNK and dampen the signal (Martin-Blanco et al., 1998). In addition, Gomez and colleagues (Gómez et al., 2005) found that *Drosophila* MKP3 functions as a negative feedback regulator of epidermal growth factor receptor-stimulated ERK signaling during wing vein development.

Mammalian genomes contain at least 11 *DUSP* genes encoding the MKPs (Alonso et al., 2004), several of which have been analyzed biochemically. Some MKPs are relatively non-specific toward different dpMAPKs in vitro. Other MKPs, however, show substrate specificity, including the structurally related cytosolic MKPs -3 (DUSP6), -X (DUSP7) and -4 (DUSP9), which inactivate dpERK in preference to other activated MAPKs (Camps et al., 2000; Keyse, 2000; Theodosiou and Ashworth, 2002). *Dusp6* (also known as *Mkp3* or *Pyst1*) transcripts can, in some circumstances, be induced in cultured cells by growth factors that stimulate the ERK pathway (Mourey et al., 1996; Muda et al., 1996a), but clues to physiologic inducers have come from embryonic expression analyses. We and others noticed that *Dusp6/Mkp3* is expressed during embryonic development of several vertebrate species in a pattern that corresponds with areas of active FGF signaling, suggesting that it

[1]Department of Human Genetics, University of Utah, 15 N 2030 E RM 2100, Salt Lake City, UT 84112-5330, USA. [2]Division of Radiobiology, University of Utah, 729 Arapeen Drive #2334, Salt Lake City, UT 84108-1218, USA.

*Present address: Department of Molecular and Human Genetics, Baylor College of Medicine, 633E, One Baylor Plaza, Houston, TX 77030, USA
†Author for correspondence (e-mail: suzi.mansour@genetics.utah.edu)

Accepted 17 October 2006

could be a conserved transcriptional target of FGF signals (Dickinson et al., 2002a; Klock and Herrmann, 2002; Eblaghie et al., 2003; Kawakami et al., 2003; Tsang et al., 2004; Gómez et al., 2005) (C.L. and S.L.M., unpublished). Indeed, ectopic FGF signals activate *Dusp6/Mkp3* transcription in chick, zebrafish and frog embryos, as well as in explanted mouse neural tube cultures; ectopic *Dusp6/Mkp3* expression reduces dpERK levels, and local siRNA, global morpholino-mediated knockdown, or dominant-negative experiments suggest roles for *Dusp6/Mkp3* in chick limb development, axial patterning of zebrafish embryos and anterior development of frog embryos, respectively (Eblaghie et al., 2003; Kawakami et al., 2003; Tsang et al., 2004; Echevarria et al., 2005; Gómez et al., 2005; Smith et al., 2005). Taken together, these results show that *Dusp6/Mkp3* can be activated by FGF signaling and suggest a negative feedback role for DUSP6/MKP3 in FGF/ERK signaling, but genetic loss-of-function data are lacking.

To address the hypothesis that mouse DUSP6/MKP3 plays a role in FGF-stimulated ERK signaling analogous to the MKPs that play clearly established negative feedback roles in regulating invertebrate MAPK signaling pathways, we studied *Dusp6/Mkp3* expression in FGFR-deficient mouse embryos and generated and analyzed a targeted loss-of-function *Dusp6/Mkp3* allele. Our data show that in mouse embryos, *Dusp6/Mkp3* transcription depends on FGF signaling and that dpERK is a physiologic DUSP6/MKP3 substrate. Furthermore, we find that loss of *Dusp6/Mkp3* leads to dominant, incompletely penetrant and variably expressive phenotypes that have features, including skeletal dwarfism, coronal craniosynostosis and hearing loss, in common with dominant gain-of-function mutations in human and mouse FGFRs.

Dusp6 is the official symbol for the mouse gene encoding MKP3 (MGI:1914853), and this nomenclature is used from here on.

MATERIALS AND METHODS

Whole-mount RNA in situ hybridization and dpERK immunohistochemistry

Whole mouse embryos isolated from timed pregnancies were hybridized with digoxigenin-labeled anti-sense RNA probes, which were detected according to Henrique et al. (Henrique et al., 1995). Stained embryos were cryoprotected and sectioned at 14 μm as described (Wright and Mansour, 2003). The *Dusp6* probe was complementary to nucleotides 1-413 of the *Dusp6* reference sequence (5′ UTR; GenBank Accession number NM_02628). The *Erm* probe was complementary to nucleotides 1309-1766 of the *Etv5* reference sequence (GenBank Accession number NM_023794). The *Fgfr1* probe was complementary to nucleotides 1-459 of the *Fgfr1* cDNA (5′ UTR; GenBank Accession number BC010200). The *Fgf8*, *Fgf10*, *Fgfr2b* and *Fgfr2c* isoform-specific and *Fgfr4* probes were generated as described (Wright et al., 2003; Wright and Mansour, 2003; Ladher et al., 2005). Whole mouse embryos were stained with antibodies directed against diphosphorylated ERK1/2 exactly as described by Corson et al. (Corson et al., 2003).

Dusp6 gene targeting

A *Dusp6*-containing lambda genomic phage was isolated from a strain 129SV/J library (Stratagene). Standard techniques were used to isolate a 6.9 kb fragment containing the entire gene and transform it into a *LacZ* knock-in gene targeting vector (see Fig. 3A). An nlsLacZSV40pA cassette was excised from a gene-trap vector (Yang et al., 1997), excluding the splice acceptor sequence, and inserted into the *Dusp6 Msc*I site in exon 1, fusing the first 56 codons of the DUSP6 open reading frame (ORF) in-frame with the βgal ORF. A self-excising *Neo*^{r} expression cassette (ACN) (Bunting et al., 1999) was placed immediately downstream of the *LacZ* gene for positive selection of targeted cell lines. In anticipation of the small possibility of spurious transcription initiation from inside the *LacZ* cassette, followed by translation initiation from an internal *Dusp6* AUG and/or the remote possibility of translation initiating downstream of the DUSP6/βGAL ORF on an SV40pA read-through transcript, we added a linker containing a stop codon in the DUSP6 frame into the *Bst*BI site in exon 3. Any hypothetical DUSP6 fragment produced from such transcripts would be missing portions of both the amino- and carboxy-terminal domains that are essential for DUSP6 activity (Camps et al., 1998; Zhou et al., 2001). The targeting construct was flanked by two different thymidine kinase expression cassettes for negative selection. The targeting DNA was linearized and electroporated into R1-45 embryonic stem (ES) cells. After selection in 380 μg/ml G-418 by weight (Invitrogen) and 2 mmol/l ganciclovir (Sigma), drug-resistant colonies were cloned and expanded. DNA isolated from each colony was screened by Southern blot hybridization using *Nde*I digestion and a 3′ flanking probe. DNAs showing the 7.0 kb targeted band were further screened by PCR with primers 376 (5′-GGTATCAGCCGCTCTGTCAC-3′) and 331 (5′-GGACACGGTT-GTCACAAGG-3′) for the presence of the stop codon in exon 3. The wild-type allele was 187 bp and the mutant (stop-containing) allele was 198 bp. DNAs from targeted cell lines that carried the stop codon were further analyzed by Southern blotting using a variety of enzymes and probes. Of 192 drug-resistant cell lines tested, 12 had a targeted insertion in the *Dusp6* locus and of these, eight also carried the stop codon.

Dusp6 mutant mouse generation and genotyping

All work with mice complied with protocols approved by the University of Utah Institutional Animal Care and Use Committee. Several correctly targeted cell lines were aggregated with C57Bl/6 morulae, cultured overnight and implanted into pseudopregnant females (Khillan and Bao, 1997). Three of these cell lines gave rise to chimeric males that transmitted the targeted allele (less the self-excising *Neo* cassette) to offspring. In subsequent crosses, the mutant and wild-type alleles were distinguished in tail or yolk sac DNA using either of two 3-primer PCR mixes. The mix containing primers 344 (5′-CTGTGTCGCTTTCCCTAACC-3′), 309 (5′-ACGCTGCTGCTGTTGC-3′) and 315 (5′-GACCGACTCTCCAC-CAGTGT-3′) produced a wild-type band of 499 bp and a mutant band of 363 bp. The mix containing primers 344 (as above), 357 (5′-CCAGG-GTTTTCCCAGTCA-3′) and 430 (5′-CTAGCTCCCCTAAGCGCAAT-3′) produced a wild-type band of 661 bp and a mutant band of 522 bp. No difference between intercross offspring produced from different targeted cell lines was immediately apparent; so one line was selected for all further analysis and backcrossing.

Mice carrying the *Fgfr1α* (*Fgfr1*^{tm1Cxd}, MGI:2153353) and *Fgfr2ΔIgIII* (*Fgfr2*^{tm1Cxd}, MGI:2153790) hypomorphic alleles were generously provided by Dr Chuxia Deng and genotyped as described (Xu et al., 1998; Xu et al., 1999).

Northern blot hybridization

Total RNA was isolated from E11.5 embryos or adult brains, mRNA was purified and 3 μg of each genotype was analyzed by northern blot hybridization according to standard protocols (Yang et al., 2001). The 448 bp 3′ UTR probe was generated by PCR amplification of mouse genomic DNA with primers 311 (5′-ACCCCTTGAGACACTGTAAGC-3′) and 329 (5′-GGGTATAGTGGAGCCAAAGAGA-3′). The 5′ UTR probe was the same as that used for in situ hybridization. The *LacZ* probe was generated by PCR amplification of plasmid DNA with primers 24 (5′-GGGTT-GTTACTCGCTCACA-3′) and 25 (5′-AAAGCGAGTGGCAACATGG-3′).

Skeleton preparation, computed tomography (CT) scanning and bone histology

To visualize the skeleton, animals were asphyxiated in CO_2, skinned, fixed in 95% ethanol, defatted in acetone and then stained with Alcian Blue 8GX and Alizarin Red S and cleared as described (Mansour et al., 1993). MicroCT scans of pups sacrificed at P10 were performed as described (Keller et al., 2004). Cranial vault measurements were made using reconstructed mid-sagittal sections. For bone histology, the proximal tibial metaphyses were stained en bloc with Villanueva bone stain, dehydrated in graded concentrations of alcohol, defatted in acetone and embedded in methyl methacrylate monomer. Longitudinal frontal sections of the tibia were cut at 4 μm. One set of sections was stained with 5% silver nitrate and counterstained with 0.5% basic fuchsin, another set of sections was stained with 0.1% Toluidine Blue O (Jee et al., 1997).

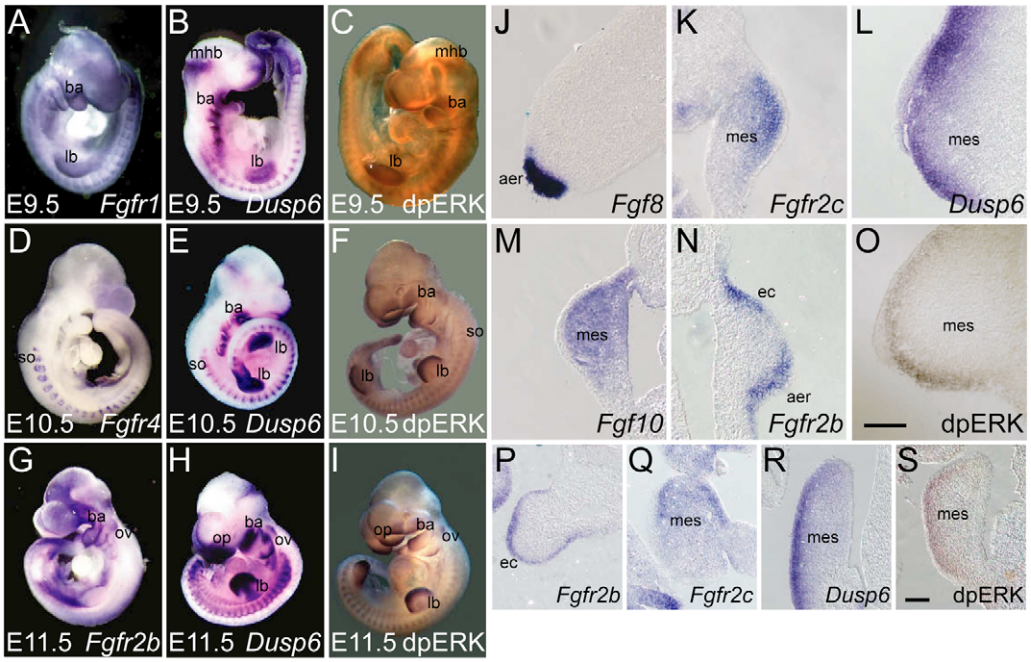

Fig. 1. *Dusp6* expression correlates with particular *Fgfr*s and with most areas of dpERK expression. (**A**,**D**,**G**) Whole-mount RNA in situ hybridization (WmISH) of mouse embryos with the *Fgfr* probes indicated at the bottom right of each panel. (**B**,**E**,**H**) WmISH of embryos with a *Dusp6* probe. (**C**,**F**,**I**) Whole-mount immunostaining of embryos with antibody directed against dpERK. Embryo age is indicated at the bottom left of each panel. (**J-S**) Transverse sections of E10-10.5 WmISH embryos illustrating potential FGF signaling pathways in the limb bud (J-O) and branchial arches (P-S). Probes are noted at the bottom left of each panel. ba, branchial arches; ec, ectoderm; lb, limb bud; mes, mesenchyme; mhb, mid-hindbrain junction; op, olfactory pit; ov, otic vesicle; so, somites. Scale bars: 100 μm in O for J-O; 100 μm in S for P-S.

Auditory brainstem response threshold measurements

Mice were anesthetized using 0.02 ml/g Avertin. Auditory brainstem response (ABR) thresholds for click (47 μs), 8 kHz, 16 kHz and 32 kHz tone pip stimuli (3000 μs, Exact Blackman envelope) were determined according to Zheng et al. (Zheng et al., 1999), using high frequency transducers controlled and analyzed by SmartEP software (Intelligent Hearing Systems).

RESULTS

Dusp6 is expressed in areas of active signaling through the FGFR/ERK pathway

It has been noted previously that in mouse, chick and zebrafish embryos, *Dusp6* (also known as *Mkp3*) is expressed in cells adjacent to those expressing *Fgf*s, particularly *Fgf*8, suggesting that transcription of *Dusp6* is regulated by FGF signals (Dickinson et al., 2002a; Klock and Herrmann, 2002; Eblaghie et al., 2003; Kawakami et al., 2003; Tsang et al., 2004). Areas of the embryo potentially competent to respond to FGF signals can be recognized by their expression of FGF receptor genes (*Fgfr*s). If *Dusp6* is a transcriptional target of FGF signaling, then it should be coexpressed with *Fgfr*s. We found that between E9.5 and 11.5, *Dusp6* expression was highly correlated with several areas of *Fgfr* expression (Fig. 1). For example, *Fgfr1* and *Dusp6* were expressed in the branchial arches and limb buds at E9.5 (Fig. 1A,B), *Fgfr4* and *Dusp6* were expressed in the somites at E10.5 (Fig. 1D,E) and *Fgfr2b* and *Dusp6* were expressed in the branchial arches and otic vesicle at E11.5 (Fig. 1G,H).

One of the intracellular pathways by which activated FGF receptors signal to the nucleus, is the ERK pathway, activation of which can be visualized by immunostaining for dpERK. Indeed, most expression domains of dpERK in E7.5-10.5 mouse embryos depend on FGF signaling (Corson et al., 2003). If *Dusp6* is a transcriptional target of FGF signaling through the ERK pathway, then it should be coexpressed with dpERK. We found that there was a striking correlation between the dpERK and *Dusp6* expression domains between E9.5 and 11.5 (Fig. 1). For example, dpERK and *Dusp6* were found in the limb buds, branchial arches and mid-hindbrain boundary at E9.5 (Fig. 1B,C), in the somites, limb buds and branchial arches at E10.5 (Fig. 1E,F) and in the limb buds, branchial arches, otic vesicles and olfactory pits at E11.5 (Fig. 1H,I).

Sections taken through the developing limb buds (Fig. 1J-O) and branchial arches (Fig. 1P-S) at E10-10.5 illustrate potential FGF signaling pathways in more detail. In the limb, the genes encoding the ligands FGF8 (Fig. 1J) and FGF10 (Fig. 1M) were expressed in the apical ectodermal ridge (aer) and mesenchyme (mes), respectively. FGF8 and FGF10 could signal to their preferred receptors, mesenchymal FGFR2c (Fig. 1K) and ectodermal FGFR2b (Fig. 1N), respectively. *Dusp6* and dpERK were primarily mesenchymal (Fig. 1L,O), suggesting that they may participate in the mesenchymal response to FGF signals. Similar FGF signaling pathways were present in the branchial arches. FGF8 and FGF10 were ectodermal and mesodermal, respectively (data not shown), whereas genes encoding their receptors, FGFR2c (Fig. 1Q) and FGFR2b (Fig. 1P), were expressed in the mesoderm and ectoderm, respectively. As in the limb bud, branchial arch *Dusp6* and dpERK were primarily mesenchymal (Fig. 1R,S). Taken together, these data show that *Dusp6* expression correlates with *Fgfr* expression domains and with sites of FGF-activated ERK signaling in the mesenchyme.

Dusp6 expression in mouse embryos depends on FGF signaling

Ectopic activation of FGF signaling in zebrafish and chick embryos or mouse neural tube explants is sufficient to induce ectopic *Dusp6* expression (Eblaghie et al., 2003; Kawakami et al., 2003; Tsang et

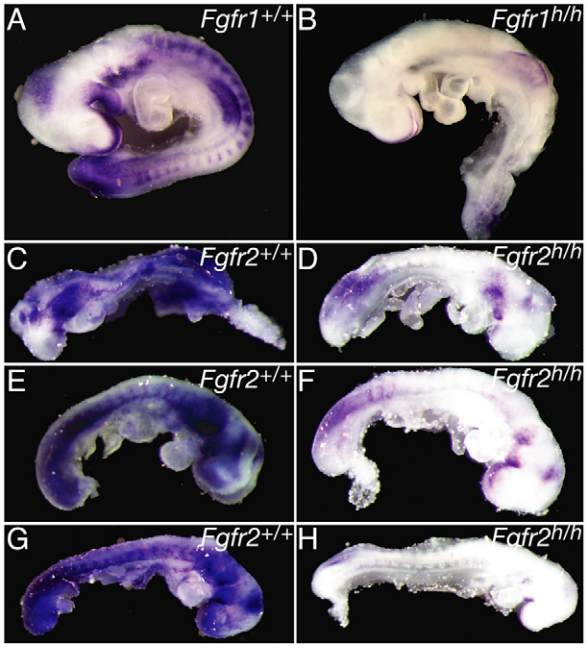

Fig. 2. *Dusp6* expression depends on signaling through FGF receptors. WmISH of wild-type and homozygous *Fgfr* hypomorphic (h) mutant littermates with a *Dusp6* probe (**A**,**B**) *Fgfr1α*, E9.5; (**C-H**) *Fgfr2ΔIgIII*, E8.5. Genotype of each embryo is indicated in the upper left of each panel.

al., 2004; Echevarria et al., 2005; Smith et al., 2005). Furthermore, genetic or physical ablation of FGF4 and FGF8 signals from the aer in mouse, chick and zebrafish embryos (Eblaghie et al., 2003; Kawakami et al., 2003), application of the FGF receptor inhibitor SU5402 to developing chick somites or mouse neural tube explants (Smith et al., 2005; Vieira and Martinez, 2005), or expression of dominant-negative FGF receptors in zebrafish embryos (Tsang et al., 2004) reduces endogenous *Dusp6* expression in the target tissue. To determine whether FGF signaling is required globally for *Dusp6* transcription in mouse embryos, we assayed *Dusp6* expression by in situ hybridization of whole mouse embryos homozygous for hypomorphic mutations in either *Fgfr1* or *Fgfr2* (Xu et al., 1998; Xu et al., 1999). *Dusp6* transcripts were severely reduced in both E9.5 *Fgfr1α* (Fig. 2A,B) and E8.5 *Fgfr2ΔIgIII* (Fig. 2C-H) homozygous embryos relative to similarly staged control embryos stained under identical conditions. These data show that *Dusp6* expression requires signaling through FGFR1 or FGFR2.

Gene targeting at the *Dusp6* locus

If *Dusp6* is a transcriptional target of FGF-activated signaling through the ERK pathway and its biochemical function is to inactivate dpERK, then ablation of *Dusp6* should lead to an increase in FGF-activated ERK signaling. Indeed, *Dusp6* morpholino-injected zebrafish embryos exhibit axial patterning phenotypes similar to those induced by ectopic *Fgf8* expression (Tsang et al., 2004). To determine the role of mouse *Dusp6*, its function was disrupted using standard gene targeting techniques to insert an in-frame *LacZ* cassette into the first coding exon and a stop codon in the third exon (Fig. 3A). Correctly targeted ES cell lines were identified by Southern blot hybridization analysis of *Nde*I-digested DNA using 3′ flanking and internal *Cre* probes (Fig. 3B). Additional digestions and probes confirmed the expected structure of the targeted allele (data not shown). Correctly targeted cell lines were further screened for the presence of the stop codon by PCR using primers flanking the newly introduced stop codon (Fig. 3C). During germline transmission of the correctly targeted, stop codon-containing allele, the *Neo* gene was automatically deleted and this was confirmed by Southern hybridization analysis (data not shown). The *LacZ* knock-in allele was designated $Dusp6^{L}$. A 3-primer PCR assay was developed to distinguish the wild type (+) and mutant (–) alleles (Fig. 3D).

To determine the efficacy of the disruption strategy, we hybridized a northern blot of E11.5 mRNAs with a *Dusp6* exon 3 3′ UTR probe (Fig. 3E). The expected ~3 kb *Dusp6* transcript and an uncharacterized, weakly expressed ~4 kb transcript were evident in wild-type and heterozygous samples, but were absent from homozygous mutant mRNA, showing that the targeting strategy effectively disrupted production of *Dusp6* mRNA. A novel, low-abundance transcript of ~7.5 kb was apparent in heterozygous and mutant samples. This is the expected size for mutant transcripts initiated at the *Dusp6* promoter and terminated at the *Dusp6*, rather than the SV40 polyadenylation signal, followed by removal of the *Dusp6* introns (see Fig. 4G,I for further hybridization data supporting this interpretation). Even if translation of this ~7.5 kb fusion mRNA could initiate at a *Dusp6* AUG codon downstream of the DUSP6/βgal ORF, a functional DUSP6 protein could not be produced from the mutant allele, as portions of both the amino- and carboxy-terminal regulatory domains required for DUSP6 activity would be absent (Camps et al., 1998; Zhou et al., 2001). Thus, the targeted allele is likely to be null.

One objective of the *LacZ* knock-in strategy was to enable a simple reporter assay for *Dusp6* expression. Surprisingly, we found that heterozygous embryos exhibited little or no βgal activity, whereas homozygous E10.5-16.5 embryos produced readily detectable βgal in a pattern that largely, though not perfectly, mimicked that of transcripts detected by whole-mount in situ hybridization in embryos of both genotypes by using either *Dusp6* 5′ UTR or *LacZ* probes (data not shown, but see Fig. 4G for northern data). This apparently post-transcriptional phenomenon is under investigation.

Dusp6 is not required for embryonic development, but has incompletely penetrant effects on dpERK, Erm and *Dusp6* levels

To assess the role of *Dusp6* in embryonic development, the F1 $Dusp6^{+/L}$ offspring of germline chimeras were intercrossed and embryos were collected and genotyped between E8.5 and 17.5. Of 1160 intercross offspring, 244 were wild type, 459 were heterozygous, 226 were homozygous mutant and 11 genotypes could not be determined. These results are consistent with a normal Mendelian distribution of wild-type and mutant alleles. No obvious abnormalities were seen in embryos of any genotype, indicating that *Dusp6* does not have a unique and visibly evident function during embryonic mouse development.

DUSP6 has a high degree of substrate specificity in vitro, dephosphorylating dpERK in preference to other MAP kinases (Groom et al., 1996; Muda et al., 1996b). To determine whether ERK signaling was perturbed in homozygous mutants, we stained whole embryos at E9.5 and 10.5 with antibodies directed against dpERK in parallel with wild-type littermate control embryos. In four out of eight homozygotes analyzed, the extent of dpERK staining was increased, particularly in the limb (Fig. 4A-C). In the remaining cases, no differences in dpERK staining between wild-type and homozygous mutant embryos could be discerned (data not shown). Thus, as predicted, DUSP6 dephosphorylates dpERK in vivo.

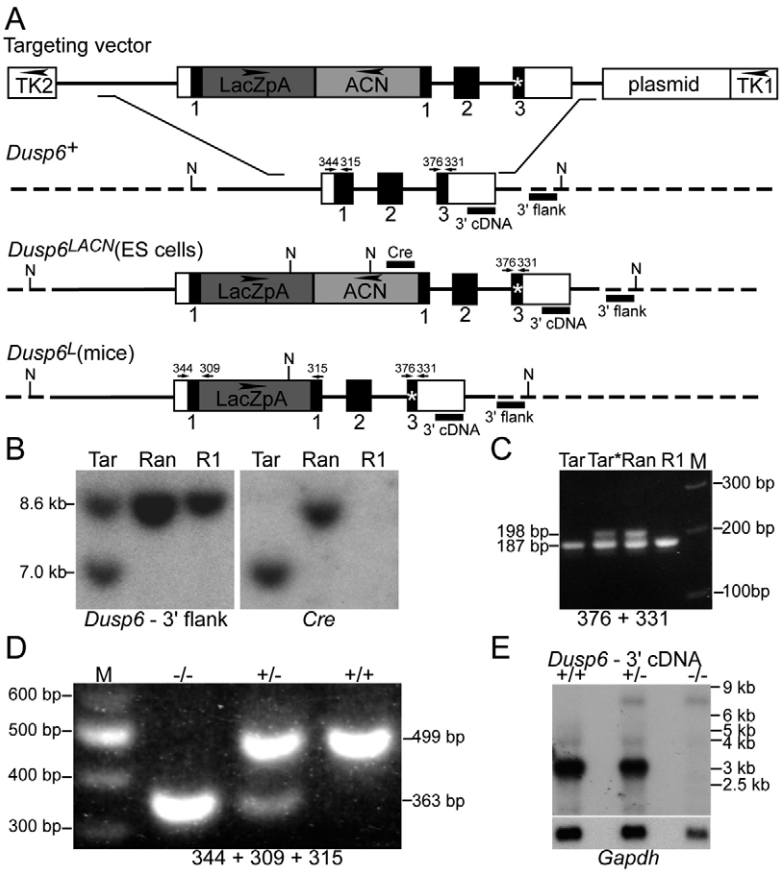

Fig. 3. Gene targeting at the *Dusp6* locus. (**A**) Structure of the linearized *Dusp6* targeting vector and depiction of the wild-type *Dusp6* allele (*Dusp6*$^{+}$), the correctly targeted mutant allele in ES cells (*Dusp6*^{LACN}) and the targeted allele found in mice following expression of CRE in germline-transmitting chimeras (*Dusp6*^{L}). Mouse genomic *Dusp6* DNA is depicted with solid thick lines; dotted lines indicate *Dusp6* genomic DNA not present in the targeting vector; open boxes indicate untranslated regions; solid boxes indicate protein coding regions. The *LacZ* gene (nls-lacZpA) is shown as a dark gray box; the Cre/Neo 'suicide cassette' (ACN) as a light gray box; the stop codon in the DUSP6 frame in exon 3 as an asterisk. Flanking thymidine kinase genes (TK1 and TK2, transcriptional orientation indicated by arrows) and the plasmid backbone are depicted as open boxes. Recognition sites for *Nde*I are indicated by 'N'; probes used for Southern analysis by black bars. Numbered arrows indicate the identity, position and directionality of primers used in PCR assays. (**B**) Southern blot hybridization assay demonstrating correct targeting of *Dusp6* in ES cells. *Nde*I-digested DNA from the R1 ES cell line (R1), a cell line with a random insertion of the targeting vector (Ran) and a targeted cell line (Tar) was probed sequentially with 3′ and Cre probes. Correctly targeted cell lines had a novel 7.0 kb fragment that hybridized with both probes. (**C**) PCR assay used to detect the stop-codon-containing insertion in exon 3. DNAs isolated from correctly targeted ES cells (Tar), a control random integrant (Ran) and wild-type cells (R1) were PCR-amplified using primers 376 and 331. Targeted cell lines (TAR*) that produced both the wild-type (187 bp) and the insertion amplicon (198 bp) were selected for germline transmission. (**D**) PCR assay used to genotype offspring of *Dusp6*$^{+/L}$ intercrosses. Tail DNAs were PCR-amplified with primers 344, 309 and 315. The mutant allele yielded a 363 bp band and the wild-type allele yielded a 499 bp band. (**E**) Northern blot hybridization of mRNA isolated from E11.5 embryos of the indicated genotypes was probed with a fragment of *Dusp6* 3′ UTR, revealing a wild-type transcript of ~3 kb in +/+ and +/– samples that was absent from the –/– sample. A minor read-through transcript of ~7.5 kb was evident in +/– and –/– samples, but due to the targeting strategy, it is incapable of encoding functional DUSP6. Rehybridization with a *Gapdh* probe is shown below.

One of the responses to activation of the ERK pathway is an increase in *Erm* (*Etv5* – Mouse Genome Informatics) transcripts (Raible and Brand, 2001; Roehl and Nüsslein-Volhard, 2001; Firnberg and Neubüser, 2002; Liu et al., 2003). To determine whether *Erm* expression was affected in *Dusp6* mutants, we subjected E10.5 embryos (nine of each genotype) to RNA in situ hybridization analysis with an *Erm* probe. After an identical staining reaction, stopped when *Erm* transcripts were just becoming evident in wild-type embryos (Fig. 4D), three out of nine heterozygous embryos had greater *Erm* expression (Fig. 4E) and three out of nine homozygotes had even more *Erm* signal (Fig. 4F). No differences from wild-type controls were apparent in the remaining heterozygous or homozygous embryos. These results confirm that inactivation of *Dusp6* can increase signaling through the ERK pathway. Furthermore, the intermediate phenotype seen in heterozygotes suggests that signaling through the ERK pathway to induce *Erm* is sensitive to the level of *Dusp6*.

If DUSP6 has a negative feedback role in ERK signaling, transcription from its promoter should be increased in *Dusp6* mutants. Northern hybridization analysis of E11.5 mRNA samples using a *Dusp6* 5′ UTR probe located upstream of the *LacZ* insertion showed a small increase in *Dusp6*-initiated transcripts present in homozygous mutant mRNA relative to wild-type and heterozygous samples (Fig. 4G; note levels of the *Gapdh* control hybridization). A second, independent comparison between genotypes showed equivalent levels of *Dusp6* 5′ UTR-containing transcripts (data not shown), presumably because multiple embryos of the same genotype were pooled to prepare the mRNA samples and the phenotype was variable. More strikingly, a similar hybridization analysis of mRNA prepared from individual adult brain samples showed a notable increase in *Dusp6* 5′ UTR-containing transcripts in homozygous mutant samples relative to wild-type and heterozygous samples (n=2 out of 4, Fig. 4H). Also as expected, in both embryonic and adult sources of mRNA, the *LacZ* probe detected transcripts from the mutant allele of ~5 kb and ~7.5 kb, reflecting production of *Dusp6/LacZ* fusion transcripts with polyadenylation probably occurring at the SV40 or *Dusp6* polyadenylation sites, respectively (Fig. 4G-I). This result shows that *Dusp6* transcription is subject to negative autoregulation.

Loss of *Dusp6* results in dominant, incompletely penetrant postnatal lethality

To determine whether *Dusp6* is required for any aspect of postnatal development, *Dusp6*$^{+/L}$ offspring of chimeric males and C57Bl/6 females were produced and offspring of these F1 *Dusp6*$^{+/L}$ intercrosses were genotyped at weaning (~4 weeks postnatal). The numbers of wild-type and heterozygous F1 progeny of the chimeras did not deviate significantly from those expected (Table 1). By contrast, of 580 F1 intercross offspring genotyped, 168 were wild type, 287 were heterozygotes and only 125 were homozygotes (Table 1), all of which appeared normal. This genotypic distribution deviated slightly, but significantly, from the Mendelian expectation

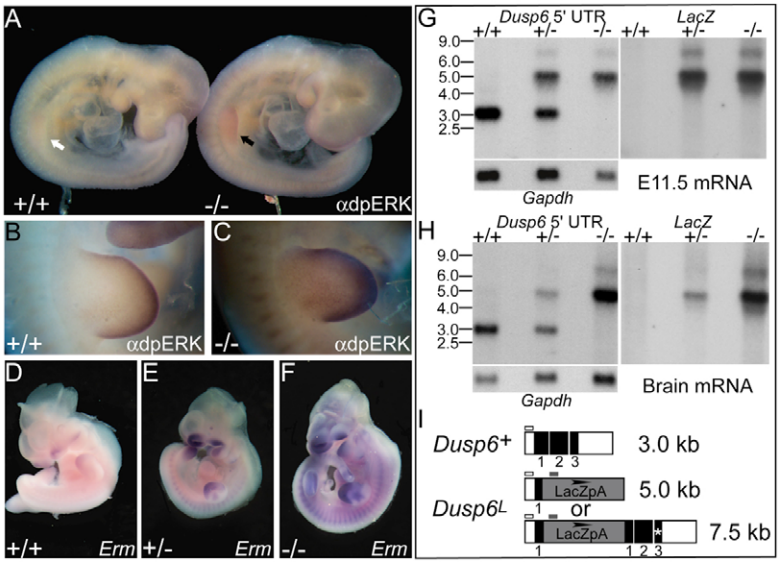

Fig. 4. DUSP6 is a negative feedback regulator of the ERK pathway. (**A-C**) Immunostaining of wild-type and *Dusp6*$^{-/-}$ embryos with anti-dpERK. (**A**) An E9.5 *Dusp6*$^{-/-}$ embryo has increased levels of dpERK in the limb (black arrow) relative to that of a wild-type embryo (white arrow). (**B**) Limb bud of wild-type E10.5 embryo. (**C**) Limb bud of *Dusp6*$^{-/-}$ embryo with increased levels of dpERK. (**D-F**) RNA in situ hybridization of E10.5 embryos shows increasing levels of *Erm* transcripts as *Dusp6* levels decrease. Genotype of each embryo is indicated in the lower left of each panel. Northern blot hybridization of mRNA isolated from pooled E11.5 embryos (**G**) or individual adult brains (**H**) of the indicated genotypes and probed sequentially with a *Dusp6* 5′ UTR probe, a *LacZ* probe and *Gapdh* shows that embryos lacking *Dusp6* have increased levels of transcripts initiated from the *Dusp6* promoter. Note that the embryonic *Gapdh* panel is identical to the one shown in Fig. 3E, because it comes from the same blot. (**I**) Diagrams of the transcripts produced by wild-type (*Dusp6*$^{+}$) and mutant (*Dusp6*^{L}) alleles and the locations of the probes (bars above transcripts) used for hybridization. Open boxes, untranslated *Dusp6* sequence; black boxes, DUSP6 coding sequence; gray box, *LacZ* cassette.

(*P*=0.04) and suggested reduced viability of homozygotes and possibly even heterozygotes. Increasing the C57Bl/6 contribution to the genetic background by crossing F1 heterozygotes to C57Bl/6 animals caused a significant reduction in the observed numbers of heterozygous offspring relative to wild type. Of 540 F1 × C57Bl/6 offspring, 309 were wild type and only 231 were heterozygous (*P*=0.00078, Table 1). The genotypic distribution of the F2 *Dusp6*$^{+/L}$ intercross offspring was even more significantly distorted than that of the F1 intercross. Among 505 total offspring, 142 were wild type, 269 were heterozygous and 94 were homozygous mutant (*P*=0.0036, Table 1). The very mixed genetic background of this intercross may explain why the heterozygous lethality seen in the backcross was not obvious. Taken together, these breeding results suggest that the *Dusp6* mutation is associated with dominant, but incompletely penetrant, postnatal lethality that is exacerbated on the C57Bl/6 background.

Loss of *Dusp6* causes skeletal dwarfism

Observations of F1 intercross litters before weaning indicated that most litters had pups that appeared smaller than their littermates after about P5. Therefore, we collected and genotyped intercross pups between P5 and P16. Pups were scored as small if their weight was less than 75% of the littermate average. An example of a small P10 heterozygote and its normally sized wild-type littermate is shown in Fig. 5A. Of 115 intercross offspring (predominantly from the F1 intercross, but including some litters from the F2 intercross), 31 were wild type (three small), 60 were heterozygous (four small), 23 were homozygous mutant (ten small) and one could not be genotyped because it was cannibalized after initial observation. This genotypic distribution was not significantly different from the Mendelian expectation, but about 40% of the P5-16 homozygotes were small. Small homozygous or heterozygous animals were not routinely observed prenatally or at weaning, suggesting that pre-weaning lethality of the subset of small heterozygous or homozygous individuals can account for the reduced number of these animals genotyped at weaning.

As small *Dusp6* mutants did not appear to have any physical impediments to feeding, such as malocclusion or cleft palate (data not shown), we examined their long bones for disturbances of the growth plate. The proximal tibia of a P14 wild-type animal had typical histology, with well-ordered chondrocytes proceeding through proliferative, hypertrophic and ossification stages (Fig. 5B,D). By contrast, the proximal tibia of a small P14 *Dusp6*$^{-/-}$ pup had severely reduced hypertrophic and ossification zones (Fig. 5C). In addition, chondrocytes in the mutant proliferating zone were disorganized; they did not form typical long straight columns of cells (Fig. 5E). This phenotype was observed in all three small mutants examined and is very similar to that of mice bearing activating mutations in FGFR3 (Brodie and Deng, 2003).

Table 1. *Dusp6* backcross and intercross genotypes

Genotype at weaning	Chimera×Bl/6	F1×Bl/6
+/+	177	309
+/–	169	231
Total	346	540
P value	0.67	0.00078*

	F1 intercross	F2 intercross
+/+	168	142
+/–	287	269
–/–	125	94
Total	580	505
P value	0.04*	0.0036*

Offspring of the indicated crosses were genotyped at weaning. *P* values were determined using the method of χ^2.
*, significant *P* values.

Loss of *Dusp6* causes craniosynostosis

Mildly activating mutations in FGFR1 and FGFR2 typically cause craniosynostoses (premature fusions of the cranial sutures) in humans and mice, and hand and foot malformations in humans. In addition, the P250R substitution in FGFR3 causes ‘non-syndromic’ craniosynostosis in humans (Zhou et al., 2000; Brodie and Deng, 2003; Chen et al., 2003; Wang et al., 2005; Wilkie, 2005). Therefore, we examined small *Dusp6*$^{+/L}$ and *Dusp6*$^{L/L}$ animals for additional phenotypes associated with activation of FGF signaling. Staining the carcasses of small P5-15 animals to reveal cartilage and bone showed coronal craniosynostosis in small heterozygous and homozygous individuals (Fig. 5G,I), but not in wild-type (Fig. 5F,H) or normally sized *Dusp6*$^{+/L}$ or *Dusp6*$^{L/L}$ pups (data not shown).

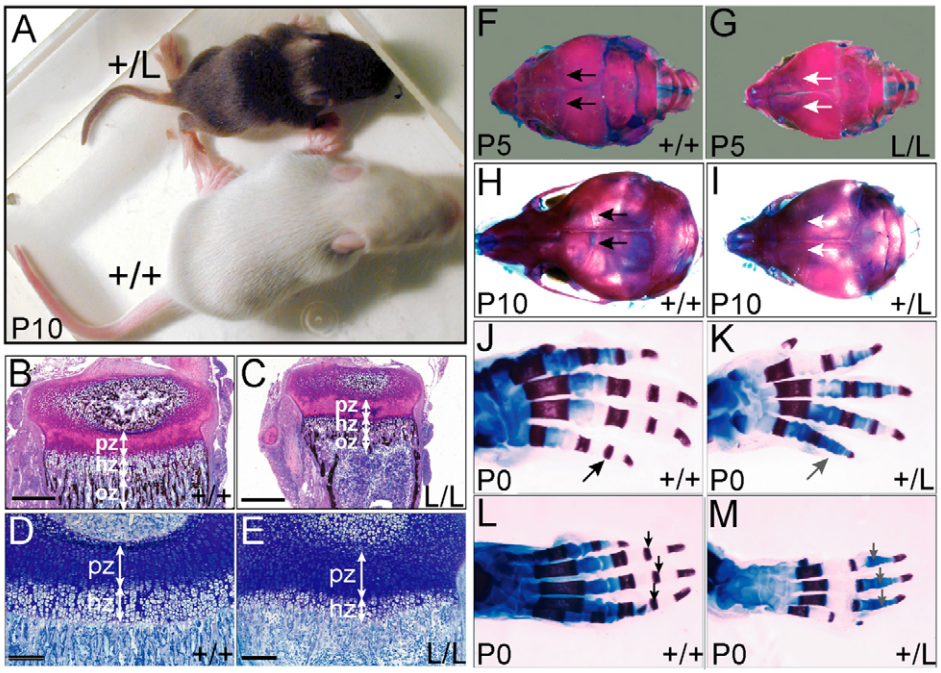

Fig. 5. Reduction or loss of *Dusp6* can result in skeletal dwarfism, altered growth plates, coronal craniosynostosis and delayed ossification of the phalanges. (**A**) Small *Dusp6*$^{+/L}$ P10 pup (+/L) and wild-type (+/+) littermate. (B-E) Frontal sections (4 μm) of undecalcified P14 proximal tibia from wild-type and small *Dusp6*$^{L/L}$ pups stained with silver nitrate and basic fuchsin. (**B**,**C**) The ossification, hypertrophic and proliferation zones are indicated. Higher magnification views of Toluidine Blue-stained sections of wild type (**D**) and mutant (**E**) growth plates. (**F-I**) Dorsal views (anterior is to the left) of Alizarin Red (bone) and Alcian Blue (cartilage)-stained skulls of P5 and P10 pups. Black arrows in F and H indicate the open coronal sutures in wild-type skulls and white arrows in G and I indicate the fused coronal sutures in small homozygous and heterozygous mutant pups, respectively. (J-M) Dorsal views of P0 and P5 control and small heterozygous or homozygous mutant autopod skeletons. (**J**,**K**) Right hands, black and gray arrows indicate the presence and absence, respectively, of the primary ossification center of the middle phalanx of the fifth digit. (**L**,**M**) Right feet, black and gray arrows indicate the presence and absence, respectively, of the primary ossification centers of the middle phalangeal ossification centers for digits 2-4. Age and genotype are indicted to the lower left and lower right of each panel, respectively. Scale bars: 0.5 mm in B,C; 0.2 mm in D,E. hz, hypertrophic zone; oz, ossification zone; pz, proliferation zone.

Furthermore, microCT scanning of small P10 *Dusp6*$^{+/L}$ and *Dusp6*$^{L/L}$ skeletons showed that the skull vault height:length and height:width ratios were significantly larger than those of the corresponding wild-type control ratios, which is consistent with mild craniosynostosis (Table 2).

By contrast, no obvious hand or foot malformations were apparent (data not shown), but the ossification sequence of the phalanges was slightly delayed in small animals. For example, at P0, the primary ossification center of the middle phalanx of the fifth digit of the hand was clearly visible in a wild-type pup but had not yet ossified in its small heterozygous littermate (Fig. 5J,K). In addition, all of the middle phalangeal ossification centers for digits 2-4 could be seen in wild-type feet but were not yet ossified in a small heterozygous littermate (Fig. 5L,M). By P5, ossification in small heterozygotes or homozygotes resembled that of wild-type littermates (data not shown). Thus, reduction or loss of *Dusp6* caused at least two phenotypes, skeletal dwarfism and craniosynostosis, which are also consequences of activated FGF signaling, but this mutation was not associated with significant distal limb malformations.

Loss of *Dusp6* causes hearing loss

Clinical descriptions of patients with dominant, activating FGFR mutations often include reports of sensorineural and/or conductive deafness (Gorlin, 2004). Therefore, we measured ABR thresholds at about 6 weeks of age in normally sized animals of all three *Dusp6* genotypes, but no significant differences between genotypes were observed (data not shown). In addition, five small intercross offspring survived to 21-28 days and could be evaluated for an ABR. Four of the five small animals had ABR thresholds that were

Table 2. MicroCT scanning measurements of wild-type and small heterozygous or homozygous mutant P10 skulls

Genotype	L (mm)	H (mm)	W (mm)	H:L	H:W	W:L
+/+ *n*=4	12.75±0.80	6.00±0.25	9.25±0.15	0.47±0.02	0.65±0.02	0.73±0.01
small +/L	11.40	6.22	8.70	0.55	0.72	0.76
small L/L	12.16	6.39	8.52	0.53	0.75	0.70

The wild-type control measurements for cranial vault measurements are presented as an average in mm ±1 s.d.
H, height; L, length; W, width.

Table 3. Auditory brainstem response threshold measurements for small *Dusp6* mutant pups

Stimulus	*Dusp6*$^{+/+}$ controls, mean dB±s.d. (*n*=13)	I607 *Dusp6*$^{+/-}$	I642 *Dusp6*$^{-/-}$	I919 *Dusp6*$^{-/-}$	I1034 *Dusp6*$^{+/-}$	I1008 *Dusp6*$^{+/-}$
L click	35.4±3.2	70*	40	60*	NR*	50*
R click	35.0±3.5	55*	40	35	NR*	25

NR, no response at maximum test level (90 dB).
*, significant difference (>2 s.d. above mean).

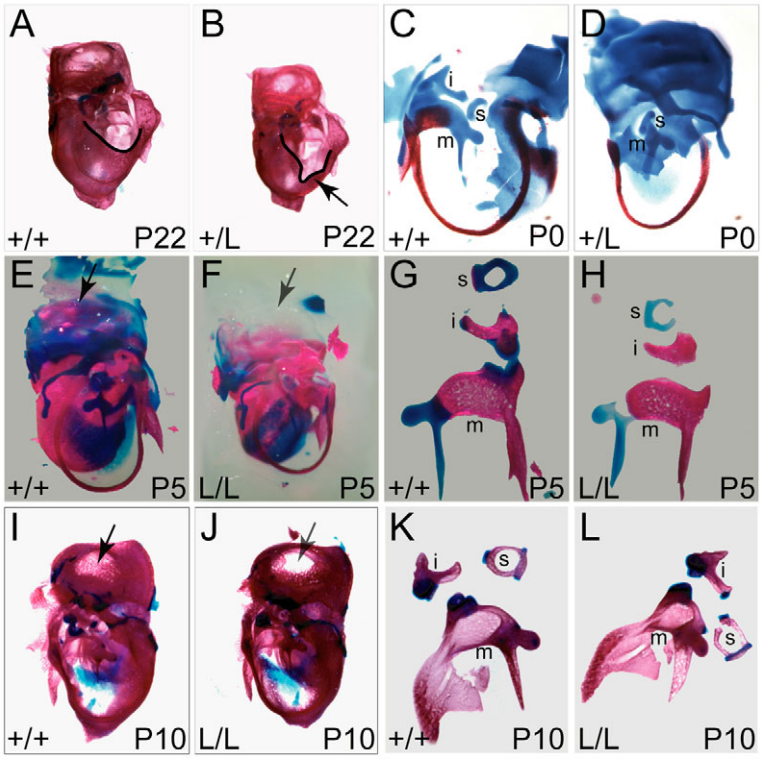

Fig. 6. Staining for bone and cartilage reveals abnormalities of the otic capsule and ossicles in mature and developing small *Dusp6*-deficient animals. (**A**,**B**) Lateral views of left temporal bones of control (A) and small heterozygous hearing-impaired (B) P22 animals. The shape of the opening to the middle ear cavity is emphasized with a black line, and an abnormal notch in the heterozygote is indicated with an arrow. (**C**,**D**) Lateral views of left ears of P0 control (C) and small heterozygous (D) P0 animals are shown with some of the cochlea dissected away to enable better visualization of the ossicles. The malleus and stapes and incus are indicated. (**E**,**F**) Lateral views of right inner ears of P5 wild-type (E) and small *Dusp6*$^{L/L}$ (F) pups. Black arrow in E indicates a normal dorsal otic capsule, and gray arrow in F indicates failure of the corresponding region of the mutant otic capsule to form Alcian Blue-positive cartilage. (**G**,**H**) Right ossicles dissected from P5 wild-type (G) and small *Dusp6*$^{L/L}$ (H) pups. All three mutant ossicles have regions in which cartilage (blue) is missing or weakly staining. (**I**,**J**) Lateral views of left temporal bones from wild-type (I) and small, *Dusp6*$^{L/L}$ (J) P10 pups. Black arrow in I indicates normal development of the dorsal otic capsule, whereas gray arrow in J indicates that the corresponding region of the mutant capsule has failed to form Alizarin Red-positive bone. (**K**,**L**) Left middle ears from wild-type (K) and small *Dusp6*$^{L/L}$ (L) P10 pups. The mutant malleus is malformed. i, incus; m, malleus; s, stapes.

significantly elevated in one or both ears relative to wild-type littermates and other similarly aged control mice (Table 3). Examination of inner ear histology from a small heterozygote (I607) with bilaterally increased ABR thresholds did not reveal any obvious abnormalities relative to a normal hearing control littermate, whereas in another small bilaterally affected heterozygote (I1034), the opening of the middle ear cavity, to which the tympanic membrane attaches, was distorted (Fig. 6A,B). That animal had ossicles that appeared normal (data not shown). Similar results were obtained for the left (affected) ear of the unilaterally affected heterozygote, I1008. Another unilaterally affected homozygote (I919) died unattended before any tissues could be recovered for analysis.

Further examination of the small homozygous or heterozygous *Dusp6* mutant skeletons revealed that, in comparison with wild-type littermates, they had variable abnormalities of the middle ear bones and otic capsule. For example, the only small pup (a heterozygote) observed and collected at P0 lacked the left incus (Fig. 6C,D). A small P5 homozygote lacked cartilage staining in the developing right otic capsule surrounding the semicircular canals (Fig. 6E,F). The right ossicles of the same P5 homozygous mutant ear were missing tissue and/or stained weakly for cartilage (Fig. 6G,H). Finally, there was a large dorsolateral hole in the left otic capsule of a small P10 homozygote (Fig. 6I,J) and the malleus from that ear was misshapen. These data suggest that the hearing loss found in the small surviving *Dusp6*-deficient pups was likely to be conductive and could be caused by developmental delays and/or malformations of the middle ear components.

DISCUSSION

To address the hypothesis that DUSP6 functions in vivo as a negative feedback regulator of MAPK signaling, we used gene targeting to disrupt mouse *Dusp6*. Homozygous mutant embryos showed variably penetrant increased levels of dpERK, the proposed DUSP6 substrate, in the limb bud, and globally increased levels of *Erm*, a transcriptional target of the ERK pathway, as well as increased transcripts initiated from the *Dusp6* promoter itself. Taken together, these molecular data are consistent with a pathway in which signals that activate ERK lead to increased transcription of *Dusp6*. The resulting DUSP6 protein then feeds back to dampen the signal by inactivating ERK.

One signal that initiates the negative feedback loop is likely to be FGF, because we found that *Dusp6* transcription depends on signaling through FGFR1 or FGFR2. Furthermore, we found that abrogation of *Dusp6* function in mice leads to variably penetrant and expressive postnatal phenotypes that are similar to some of the features of ectopic FGF ligand expression or dominant activating mutations in FGFRs, which are major inputs into the ERK pathway (Powers et al., 2000; Tsang and Dawid, 2004; Eswarakumar et al., 2005). Beginning around P5, affected *Dusp6* mutants were small, exhibited coronal craniosynostosis and middle ear and otic capsule malformations, and affected individuals that survived past P21 frequently had uni- or bilateral hearing loss.

Skeletal dwarfism manifesting in the early postnatal period is also characteristic to various extents of mice carrying *Fgf2*- or *Fgf9*-expressing transgenes (reviewed by Ornitz and Marie, 2002), and of knock-in mice carrying the Apert syndrome equivalent mutation (FGFR2S252W) (Chen et al., 2003; Wang et al., 2005), and all of the characterized FGFR3 syndromic gain-of-function mutations (Brodie and Deng, 2003). In addition, osteoglophonic dysplasia, which can be caused by any of several activating mutations in *FGFR1* (White et al., 2005), is characterized by short stature. In general, the more strongly activating receptor mutations lead to the strongest dwarfing phenotypes (Ornitz and Marie, 2002; Chen and Deng, 2005). This is consistent with the idea that FGF signaling limits endochondral bone growth and that inactivating mutations in negative regulators of FGF signaling, such as *Spred2* (Bundschu et al., 2005) or *Dusp6*, lead to increases in FGF signaling and decreased bone growth. The bone histology of small *Dusp6* mutants (reduced hypertrophic and ossification zones, disorganized proliferation zone) is more similar to

that of mice with *Fgfr3* gain-of-function mutations (e.g. Li et al., 1999) than to the Apert knock-in models, which in one case showed a slightly reduced proliferation zone (Chen et al., 2003) and in the other subtle irregularity of the hypertrophic zone (Wang et al., 2005). This suggests that DUSP6 is more likely to regulate signaling downstream of FGFR3 than of FGFR2 in the growth plate. It would be interesting to make similar comparisons of growth plate histology when a mouse model of osteoglophonic dysplasia is produced.

The craniosynostosis seen in *Dusp6* mutants is also likely to be FGF-mediated, as similar phenotypes are seen consequent to ectopic *Fgf2* expression or retrovirally mediated increases in *Fgf3* and *Fgf4* expression. In addition, many of the models of FGF receptor activation have more severe craniosynostoses, in some instances involving the coronal as well as the interfrontal and sagittal sutures (reviewed by Ornitz and Marie, 2002; Chen and Deng, 2005), than do affected *Dusp6* mutants, in which only the coronal suture is affected. Suture formation is regulated by opposing FGF signaling pathways that control the balance of cellular proliferation (through FGFR2) and differentiation (through FGFR1) (Iseki et al., 1999). Thus, it is conceivable that *Dusp6* has differential effects on the two pathways, perhaps regulating signaling through FGFR1 rather than through FGFR2 in the developing calvarium.

No information on middle ear or otic capsule morphology or auditory status is available for any of the mouse *Fgf* or *Fgfr* gain-of-function mutations, but the common findings of hearing loss and otopathology in Apert, Pfeiffer, Crouzon and Muenke syndrome patients (Gorlin, 2004) and the mouse *Dusp6* mutant phenotype suggest that these pathologies may yet be found in the mouse models as well. Apert and Pfeiffer syndromes are characterized by limb malformations (syndactyly and broad first digits, respectively) (Muenke and Wilkie, 2000; Wilkie, 2005), but no such malformations were apparent in the small *Dusp6* mutants. This may not be surprising, as none of the mouse models for these FGFR1 and FGFR2 syndromes have limb findings, potentially reflecting slight differences in the regulation of FGF signaling between mice and humans.

Taken together, the *Dusp6* mutant phenotypes we observed do not precisely mimic any particular mouse *Fgfr* gain-of-function mutation, suggesting the possibility that *Dusp6* is downstream of more than one FGFR, but that it does not serve as a negative feedback regulator of all FGF signaling events. Our finding that hypomorphic mutations in either *Fgfr1* or *Fgfr2* reduce, but do not entirely eliminate, *Dusp6* expression at early embryonic stages further supports this idea. Genetic interaction studies between the *Dusp6* mutant allele and various *Fgf* or *Fgfr* mutations could be used to address this hypothesis and learn which specific FGF signaling events are subject to regulation by DUSP6. Indeed, our preliminary studies suggest that loss of *Dusp6* exacerbates the small size and lethality of the $Fgfr1^{P250R}$ allele. Whether this effect is a result of changes to craniofacial or limb skeletal elements or both is currently under investigation.

The variable penetrance of the embryonic molecular and postnatal morphologic phenotypes resulting from *Dusp6* loss, and the absence of discernible morphologic changes in the mutant embryos, suggest that there could be redundant ERK phosphatases that compensate to some extent for *Dusp6*. These may or may not be part of a negative feedback loop regulating ERK. DUSP7 and DUSP9 are both relatively ERK-specific in vitro (Dowd et al., 1998; Dickinson et al., 2002b), and their transcripts have some areas of overlap with *Dusp6*, particularly in the developing limb buds and branchial arches (data not shown) (Dickinson et al., 2002b). The *Dusp7* mutant phenotype has not yet been reported, but mutation of the X-linked *Dusp9* gene leads to failure of placental development and consequent lethality. Tetraploid rescued embryos develop normally, however (Christie et al., 2005). Thus, conditional *Dusp9* (and *Dusp7*) alleles will have to be generated in order to assess potential redundancy with *Dusp6*.

Finally, the similarity between the *Dusp6* mutant phenotypes and those of humans with activating FGFR mutations suggests that mutations in *DUSP6* or other negative regulators of FGF signaling, such as *SPRY* genes, SPRED genes or *SEF* (*IL17RD* – Human Gene Nomenclature Database), or indeed other *DUSP* genes, are good candidates for molecularly unexplained cases of FGFR-like syndromes. Furthermore, the increasing lethality of the *Dusp6* mutation as the allele was backcrossed to C57Bl/6 shows that there are likely to be genes that interact with *Dusp6* and suggests that genetic variation among negative regulators of FGF signaling is a potential source of modifiers of the variable expressivity of human FGFR mutations.

We are very grateful to Drs Mario Capecchi for providing an aliquot of R1-45 ES cells and the TK1+TK2 vector, Chuxia Deng for providing mice carrying the *Fgfr1α* and *Fgfr2ΔIgIII* alleles, Charles Keller for carrying out the microCT scans, Webster Jee for assistance with the bone histology and Lisa Urness for critiquing the manuscript. Xiaofen Wang provided excellent technical assistance with mouse production; Albert Noyes generously provided the dpERK data for Fig. 1C; and Samantha Covington generated the plasmid bearing the *Fgfr1* 5′ UTR fragment. This work was supported by grants from the NIH/NIDCD: R01DC02043 and R01DC04185, from the Deafness Research Foundation, and from the Children's Health Research Center. D.A.S. was a Primary Children's Medical Foundation Scholar.

References

Alonso, A., Sasin, J., Bottini, N., Friedberg, I., Friedberg, I., Osterman, A., Godzik, A., Hunter, T., Dixon, J. and Mustelin, T. (2004). Protein tyrosine phosphatases in the human genome. *Cell* **117**, 699-711.

Brodie, S. G. and Deng, C. X. (2003). Mouse models orthologous to FGFR3-related skeletal dysplasias. *Pediatr. Pathol. Mol. Med.* **22**, 87-103.

Bundschu, K., Knobeloch, K. P., Ullrich, M., Schinke, T., Amling, M., Engelhardt, C. M., Renné, T., Walter, U. and Schuh, K. (2005). Gene disruption of Spred-2 causes dwarfism. *J. Biol. Chem.* **280**, 28572-28580.

Bunting, M., Bernstein, K. E., Greer, J. M., Capecchi, M. R. and Thomas, K. R. (1999). Targeting genes for self-excision in the germ line. *Genes Dev.* **13**, 1524-1528.

Camps, M., Nichols, A., Gillieron, C., Antonsson, B., Muda, M., Chabert, C., Boschert, U. and Arkinstall, S. (1998). Catalytic activation of the phosphatase MKP-3 by ERK2 mitogen-activated protein kinase. *Science* **280**, 1262-1265.

Camps, M., Nichols, A. and Arkinstall, S. (2000). Dual specificity phosphatases: a gene family for control of MAP kinase function. *FASEB J.* **14**, 6-16.

Chen, L. and Deng, C. X. (2005). Roles of FGF signaling in skeletal development and human genetic diseases. *Front. Biosci.* **10**, 1961-1976.

Chen, L., Li, D., Li, C., Engel, A. and Deng, C. X. (2003). A Ser250Trp substitution in mouse fibroblast growth factor receptor 2 (Fgfr2) results in craniosynostosis. *Bone* **33**, 169-178.

Chen, Z., Gibson, T. B., Robinson, F., Silvestro, L., Pearson, G., Xu, B., Wright, A., Vanderbilt, C. and Cobb, M. H. (2001). MAP kinases. *Chem. Rev.* **101**, 2449-2476.

Christie, G. R., Williams, D. J., MacIsaac, F., Dickinson, R. J., Rosewell, I. and Keyse, S. M. (2005). The dual-specificity protein phosphatase DUSP9/MKP-4 is essential for placental function but is not required for normal embryonic development. *Mol. Cell. Biol.* **25**, 8323-8333.

Cohen, J. M. M. (2004). FGFs/FGFRs and associated disorders. In *Inborn Errors of Development* (eds C. J. Epstein, J. D. Erickson and A. Wynshaw-Boris), pp. 380-400. New York: Oxford University Press.

Corson, L. B., Yamanaka, Y., Lai, K. M. and Rossant, J. (2003). Spatial and temporal patterns of ERK signaling during mouse embryogenesis. *Development* **130**, 4527-4537.

Dickinson, R. J., Eblaghie, M. C., Keyse, S. M. and Morriss-Kay, G. M. (2002a). Expression of the ERK-specific MAP kinase phosphatase *PYST1/MKP3* in mouse embryos during morphogenesis and early organogenesis. *Mech. Dev.* **113**, 193-196.

Dickinson, R. J., Williams, D. J., Slack, D. N., Williamson, J., Seternes, O. M. and Keyse, S. M. (2002b). Characterization of a murine gene encoding a developmentally regulated cytoplasmic dual-specificity mitogen-activated protein kinase phosphatase. *Biochem. J.* **364**, 145-155.

Dowd, S., Sneddon, A. A. and Keyse, S. M. (1998). Isolation of the human genes encoding the Pyst1 and Pyst2 phosphatases: characterisation of Pyst2 as a

cytosolic dual-specificity MAP kinase phosphatase and its catalytic activation by both MAP and SAP kinases. *J. Cell Sci.* **111**, 3389-3399.
Eblaghie, M. C., Lunn, J. S., Dickinson, R. J., Münsterberg, A. E., Sanz-Ezquerro, J. J., Farrell, E. R., Mathers, J., Keyse, S. M., Storey, K. and Tickle, C. (2003). Negative feedback regulation of FGF signaling levels by Pyst1/MKP3 in chick embryos. *Curr. Biol.* **13**, 1009-1018.
Echevarria, D., Martinez, S., Marques, S., Lucas-Teixeira, V. and Belo, J. A. (2005). Mkp3 is a negative feedback modulator of Fgf8 signaling in the mammalian isthmic organizer. *Dev. Biol.* **277**, 114-128.
Eswarakumar, V. P., Lax, I. and Schlessinger, J. (2005). Cellular signaling by fibroblast growth factor receptors. *Cytokine Growth Factor Rev.* **16**, 139-149.
Firnberg, N. and Neubüser, A. (2002). FGF signaling regulates expression of *Tbx2*, *Erm*, *Pea3*, and *Pax3* in the early nasal region. *Dev. Biol.* **247**, 237-250.
Gómez, A. R., López-Varea, A., Molnar, C., de la Calle-Mustienes, E., Ruiz-Gómez, M., Gómez-Skarmeta, J. L. and de Celis, J. F. (2005). Conserved cross-interactions in *Drosophila* and *Xenopus* between Ras/MAPK signaling and the dual-specificity phosphatase MKP3. *Dev. Dyn.* **232**, 695-708.
Gorlin, R. J. (2004). Genetic hearing loss associated with musculoskeletal disorders. In *Hereditary Hearing Loss and Its Syndromes* (eds H. V. Toriello, W. Reardon and R. J. Gorlin), pp. 166-266. New York: Oxford University Press.
Groom, L. A., Sneddon, A. A., Alessi, D. R., Dowd, S. and Keyse, S. M. (1996). Differential regulation of the MAP, SAP and RK/p38 kinases by Pyst1, a novel cytosolic dual-specificity phosphatase. *EMBO J.* **15**, 3621-3632.
Henrique, D., Adam, J., Myat, A., Chitnis, A., Lewis, J. and Ish-Horowicz, D. (1995). Expression of a Delta homologue in prospective neurons in the chick. *Nature* **375**, 787-790.
Iseki, S., Wilkie, A. O. and Morriss-Kay, G. M. (1999). *Fgfr1* and *Fgfr2* have distinct differentiation- and proliferation-related roles in the developing mouse skull vault. *Development* **126**, 5611-5620.
Itoh, N. and Ornitz, D. M. (2004). Evolution of the *Fgf* and *Fgfr* gene families. *Trends Genet.* **20**, 563-569.
Jee, W. S. S., Li, X. J., Inoue, J., Jee, K. W., Haba, T., Ke, H. Z., Setterberg, R. B. and Ma, Y. F. (1997). Histomorphometric assay of the growing bone. In *Handbook of Bone Morphology* (ed. H. E. Takahashi), pp. 87-112. Niigata, Japan: Nishimura.
Kawakami, Y., Rodriguez-León, J., Koth, C. M., Büscher, D., Itoh, T., Raya, A., Ng, J. K., Esteban, C. R., Takahashi, S., Henrique, D. et al. (2003). MKP3 mediates the cellular response to FGF8 signalling in the vertebrate limb. *Nat. Cell Biol.* **5**, 513-519.
Keller, C., Arenkiel, B. R., Coffin, C. M., El-Bardeesy, N., DePinho, R. A. and Capecchi, M. R. (2004). Alveolar rhabdomyosarcomas in conditional *Pax3:Fkhr* mice: cooperativity of Ink4a/ARF and Trp53 loss of function. *Genes Dev.* **18**, 2614-2626.
Keyse, S. M. (2000). Protein phosphatases and the regulation of mitogen-activated protein kinase signalling. *Curr. Opin. Cell Biol.* **12**, 186-192.
Khillan, J. S. and Bao, Y. (1997). Preparation of animals with a high degree of chimerism by one-step coculture of embryonic stem cells and preimplantation embryos. *Biotechniques* **22**, 544-549.
Klock, A. and Herrmann, B. G. (2002). Cloning and expression of the mouse dual-specificity mitogen-activated protein (MAP) kinase phosphatase *Mkp3* during mouse embryogenesis. *Mech. Dev.* **116**, 243-247.
Ladher, R. K., Wright, T. J., Moon, A. M., Mansour, S. L. and Schoenwolf, G. C. (2005). FGF8 initiates inner ear induction in chick and mouse. *Genes Dev.* **19**, 603-613.
Li, C., Chen, L., Iwata, T., Kitagawa, M., Fu, X. Y. and Deng, C. X. (1999). A Lys644Glu substitution in fibroblast growth factor receptor 3 (FGFR3) causes dwarfism in mice by activation of STATs and ink4 cell cycle inhibitors. *Hum. Mol. Genet.* **8**, 35-44.
Liu, Y., Jiang, H., Crawford, H. C. and Hogan, B. L. (2003). Role for ETS domain transcription factors Pea3/Erm in mouse lung development. *Dev. Biol.* **261**, 10-24.
Mansour, S. L., Goddard, J. M. and Capecchi, M. R. (1993). Mice homozygous for a targeted disruption of the proto-oncogene *int-2* have developmental defects in the tail and inner ear. *Development* **117**, 13-28.
Martin-Blanco, E., Gampel, A., Ring, J., Virdee, K., Kirov, N., Tolkovsky, A. M. and Martinez-Arias, A. (1998). *puckered* encodes a phosphatase that mediates a feedback loop regulating JNK activity during dorsal closure in *Drosophila*. *Genes Dev.* **12**, 557-570.
Mourey, R. J., Vega, Q. C., Campbell, J. S., Wenderoth, M. P., Hauschka, S. D., Krebs, E. G. and Dixon, J. E. (1996). A novel cytoplasmic dual specificity protein tyrosine phosphatase implicated in muscle and neuronal differentiation. *J. Biol. Chem.* **271**, 3795-3802.
Muda, M., Boschert, U., Dickinson, R., Martinou, J. C., Martinou, I., Camps, M., Schlegel, W. and Arkinstall, S. (1996a). MKP-3, a novel cytosolic protein-tyrosine phosphatase that exemplifies a new class of mitogen-activated protein kinase phosphatase. *J. Biol. Chem.* **271**, 4319-4326.
Muda, M., Theodosiou, A., Rodrigues, N., Boschert, U., Camps, M., Gillieron, C., Davies, K., Ashworth, A. and Arkinstall, S. (1996b). The dual specificity phosphatases M3/6 and MKP-3 are highly selective for inactivation of distinct mitogen-activated protein kinases. *J. Biol. Chem.* **271**, 27205-27208.
Muenke, M. and Wilkie, A. O. M. (2000). Craniosynostosis syndromes. In *The Metabolic and Molecular Bases of Inherited Disease* (eds C. R. Scriver, A. L. Beaudet, D. Valle and W. S. Sly), pp. 6117-6146. New York: McGraw-Hill.
Ornitz, D. M. and Marie, P. J. (2002). FGF signaling pathways in endochondral and intramembranous bone development and human genetic disease. *Genes Dev.* **16**, 1446-1465.
Powers, C. J., McLeskey, S. W. and Wellstein, A. (2000). Fibroblast growth factors, their receptors and signaling. *Endocr. Relat. Cancer* **7**, 165-197.
Raible, F. and Brand, M. (2001). Tight transcriptional control of the ETS domain factors Erm and Pea3 by Fgf signaling during early zebrafish development. *Mech. Dev.* **107**, 105-117.
Roehl, H. and Nüsslein-Volhard, C. (2001). Zebrafish *pea3* and *erm* are general targets of FGF8 signaling. *Curr. Biol.* **11**, 503-507.
Smith, T. G., Sweetman, D., Patterson, M., Keyse, S. M. and Münsterberg, A. (2005). Feedback interactions between MKP3 and ERK MAP kinase control *scleraxis* expression and the specification of rib progenitors in the developing chick somite. *Development* **132**, 1305-1314.
Theodosiou, A. and Ashworth, A. (2002). MAP kinase phosphatases. *Genome Biol.* **3**, REVIEWS3009.
Thisse, B. and Thisse, C. (2005). Functions and regulations of fibroblast growth factor signaling during embryonic development. *Dev. Biol.* **287**, 390-402.
Tsang, M. and Dawid, I. B. (2004). Promotion and attenuation of FGF signaling through the Ras-MAPK pathway. *Sci. STKE* **2004**, pe17.
Tsang, M., Maegawa, S., Kiang, A., Habas, R., Weinberg, E. and Dawid, I. B. (2004). A role for MKP3 in axial patterning of the zebrafish embryo. *Development* **131**, 2769-2779.
Vieira, C. and Martinez, S. (2005). Experimental study of MAP kinase phosphatase-3 (*Mkp3*) expression in the chick neural tube in relation to Fgf8 activity. *Brain Res. Brain Res. Rev.* **49**, 158-166.
Wang, Y., Xiao, R., Yang, F., Karim, B. O., Iacovelli, A. J., Cai, J., Lerner, C. P., Richtsmeier, J. T., Leszl, J. M., Hill, C. A. et al. (2005). Abnormalities in cartilage and bone development in the Apert syndrome FGFR2(+/S252W) mouse. *Development* **132**, 3537-3548.
White, K. E., Cabral, J. M., Davis, S. I., Fishburn, T., Evans, W. E., Ichikawa, S., Fields, J., Yu, X., Shaw, N. J., McLellan, N. J. et al. (2005). Mutations that cause osteoglophonic dysplasia define novel roles for FGFR1 in bone elongation. *Am. J. Hum. Genet.* **76**, 361-367.
Wilkie, A. O. (2005). Bad bones, absent smell, selfish testes: the pleiotropic consequences of human FGF receptor mutations. *Cytokine Growth Factor Rev.* **16**, 187-203.
Wright, T. J. and Mansour, S. L. (2003). *Fgf3* and *Fgf10* are required for mouse otic placode induction. *Development* **130**, 3379-3390.
Wright, T. J., Hatch, E. P., Karabagli, H., Karabagli, P., Schoenwolf, G. C. and Mansour, S. L. (2003). Expression of mouse fibroblast growth factor and fibroblast growth factor receptor genes during early inner ear development. *Dev. Dyn.* **228**, 267-272.
Xu, X., Weinstein, M., Li, C., Naski, M., Cohen, R. I., Ornitz, D. M., Leder, P. and Deng, C. (1998). Fibroblast growth factor receptor 2 (FGFR2)-mediated reciprocal regulation loop between FGF8 and FGF10 is essential for limb induction. *Development* **125**, 753-765.
Xu, X., Li, C., Takahashi, K., Slavkin, H. C., Shum, L. and Deng, C. X. (1999). Murine fibroblast growth factor receptor 1alpha isoforms mediate node regression and are essential for posterior mesoderm development. *Dev. Biol.* **208**, 293-306.
Yang, W., Musci, T. S. and Mansour, S. L. (1997). Trapping genes expressed in the developing mouse inner ear. *Hear. Res.* **114**, 53-61.
Yang, W., Li, C. and Mansour, S. L. (2001). Impaired motor coordination in mice that lack punc. *Mol. Cell. Biol.* **21**, 6031-6043.
Zhan, X. L., Deschenes, R. J. and Guan, K. L. (1997). Differential regulation of FUS3 MAP kinase by tyrosine-specific phosphatases PTP2/PTP3 and dual-specificity phosphatase MSG5 in *Saccharomyces cerevisiae*. *Genes Dev.* **11**, 1690-1702.
Zheng, Q. Y., Johnson, K. R. and Erway, L. C. (1999). Assessment of hearing in 80 inbred strains of mice by ABR threshold analyses. *Hear. Res.* **130**, 94-107.
Zhou, B., Wu, L., Shen, K., Zhang, J., Lawrence, D. S. and Zhang, Z. Y. (2001). Multiple regions of MAP kinase phosphatase 3 are involved in its recognition and activation by ERK2. *J. Biol. Chem.* **276**, 6506-6515.
Zhou, Y. X., Xu, X., Chen, L., Li, C., Brodie, S. G. and Deng, C. X. (2000). A Pro250Arg substitution in mouse Fgfr1 causes increased expression of Cbfa1 and premature fusion of calvarial sutures. *Hum. Mol. Genet.* **9**, 2001-2008.